Vietnam Journal of Catalysis and Adsorption
Tạp chí xúc tác và hấp phụ Việt Nam

http://chemeng.hust.edu.vn/jca/

A comparative study on the catalytic activities of the $SrTiO_3$ perovskite and oxide CuO-ZnO mixed oxides for the oxidative coupling of methane

Hung Nguyen Thanh[1], Phuong Pham Thi Mai[2], To Dang Thi[1], Thang Le Minh[1,*]

[1] *School of Chemical Engineering, Hanoi University of Science and Technology, Viet Nam*
[2] *Advanced Institue of Science and Technology, Hanoi University of Science and Technology, Viet Nam*
**Email: thang.leminh@hust.edu.vn*

ARTICLE INFO

Received: 19/12/2021
Accepted: 20/3/2022
Published: 05/4/2022

Keywords:

$SrTiO_3$, CuO-ZnO, OCM, sol-gel

ABSTRACT

In this study, $SrTiO_3$ catalyst was prepared by sol-gel method and CuO-ZnO by co-precipitation for oxidative coupling of methane (OCM). The results showed that the conversion rate in the $SrTiO_3$ sample was high (about 35%) at 850 °C, and the product C_2H_4 with an yield of 0.12%. Several modern analytical methods such as XRD, BET, TPx, SEM have been characterized. The XRD results showed a stable phase structure and high crystallinity with both samples. NH_3-TPD recorded weak acid centers on $SrTiO_3$, leading to coke formation on the impact surface. H_2-TPR and O_2-TPD express the redox of CuO-ZnO, resulting in a deep oxidation product of CO_2. Factors affecting the ratio of C_2H_6 and C_2H_4 were also considered.

Introduction

As a significant component of natural gas, shale gas, and gas hydrates, methane is a cheap hydrocarbon resource that can be converted into valuable chemicals by natural and chemical processes of indirect learning. However, syngas production by conversion requires high temperatures and large amounts of energy, which makes indirect conversion methods not cost-effective [2,3]. Typical for the direct method is the (OCM) for the direct conversion of methane to olefins and bowls of paraffin, which has been studied for many decades [1]. OCM reactions generally involve the formation of methyl radicals (CH_3*) through the separation of hydrogen from methane by the active surface oxygen species available on the surface of the oxide catalyst [4,5].

The methyl radicals then pair up in the gas phase to form ethane (C_2H_6), finally dehydrogenated to form ethylene (C_2H_4). However, this long-lived reaction is restricted to economically low C_2 yields, primarily for reasons that include: (1) A catalyst capable of activating CH_4 also stimulates Activated C_2H_6 is generated at a similar rate, thus producing a highly thermodynamic CO_x gas stable [6, 7]; (2) Recharge of oxygen sites on the drum surface generated by gas-phase oxygen sometimes leads to adsorbed oxygen species that facilitate CO_x formation as an undesirable scheme (3) In addition, the diffusive dispersion of the bulk lattice of oxygen to the oxide surface is usually very slow. It thus leads to low overall activity, especially in the absence of a potential gas phase (4) flow of oxygen. Methane combustion is often high due to the required temperature (above 800 °C) of the OCM reaction [8].

https://doi.org/10.51316/jca.2022.060

Among the various catalysts reported for OCM, perovskite (described as ABO_3 where A stands for lanthanum, alkali, or alkaline earth metals, and B denotes transition metal) has been proposed [9, 10]. One of the catalysts that confirmed its good catalytic activity is $SrTiO_3$, with high C_2 selectivity and large CH_4 conversion [11, 12]. However, there have not been many studies to clarify the advantages of this type of catalyst over simple catalyst systems such as mixtures of oxides. Therefore, this study compares catalytic properties such as phase composition, surface charge, redox properties, and catalytic activity of $SrTiO_3$ and CuO-ZnO catalysts under reaction conditions with temperatures from 750 to 850 ^oC is summarized.

Experimental

Materials

Copper nitrate ($Cu(NO_3)_2.3H_2O$, Sigma Aldrich) and zinc nitrate ($Zn(NO_3)_2.6H_2O$, Sigma Aldrich), Sodium hydroxide (NaOH) were employed as metal precursors. Ethylene glycol ($HOCH_2CH_2OH$, 99.8%), Strontium nitrate ($Sr(NO_3)_2$, Sigma Aldrich), citric acid ($C_6H_6O_8$, 99.5%), Titanium isopropoxide ($Ti[OCH(CH_3)_2]_4$ 97%, Sigma Aldrich) were used to prepare $SrTiO_3$.

Preparation of catalyst

CuO-ZnO catalysts were prepared by a conventional co-precipitation method. Sodium hydroxide (NaOH) was used as a precipitation agent. Firstly, Zinc nitrate (14.11g) was dissolved in 100 mL of distilled water. Then a suitable quantity of $Cu(NO_3)_2$ was added to the above mixture to obtain Solution A, with a molar ratio of Cu/ Zn =30%. NaOH (5g) was dissolved in 50 mL of distilled water (Solution B). Solution B was simultaneously added dropwise into Solution A, and an amount of distilled water was added to give a system volume of 200 mL. The mixture was maintained by stirring on a magnetic stirrer for one h at 300 pm. The resulting precipitate was vacuum filtered, washed with distilled water and ethanol 4-5 times, and dried at 90 °C for 12 h. Finally, the dry sample was pulverized and calcined at 900 °C for three h at a heating rate of 3 °C/min to obtain a CuO-ZnO catalyst.

Titanium isopropoxide (9.15 mL) was dissolved in ethylene glycol (26.9 mL) and stirred at 60 °C for 30 min to obtain a clear solution. DI water (20 mL) was added to titanium isopropoxide and ethylene glycol solution stirred at 80 °C for another one h. The solution is now cloudy white. After this time, citric acid (25.8 g) was added to the solution at 80 °C to give a clear solution of yellow color during vigorous stirring. $Sr(NO_3)_2$ (5.3 g) was added to the above solution and continued stirring until a viscous gel was formed. The gel was then air-dried at 200 °C for 12 hours, and the resulting dry powder was calcined in air at 900 °C for 5 hours at a rate of 3 °C/min.

Characterization

The crystalline phase of samples was investigated by X-ray powder diffraction (XRD). XRD patterns were obtained by using Bruker Axs D8 Advance XRD-diffractometer (Germany) with Cu K_α irradiation (40kV, 40 mA). The morphology of the catalyst was captured by Scanning Electronic Spectroscopy (SEM) on Novanosem 450 (FEI). The textural properties were measured via N_2 adsorption/desorption isotherms using a Micromeritics (Gemini VII analyzer). The specific surface area, pore volume, and pore diameter were obtained using the Brunauer-Emmett-Teller (BET) method. To determine the reducing capacity of the oxide surface and the inhomogeneity of the reducing surface, the H_2-TPR measurement is used. Temperature-programmed oxygen desorption (O_2-TPD) is analyzed to quantify and classify oxygen-containing groups on the material's surface. The TPx method was analyzed using Micromeritics Auto Chem II 2920 instrument.

Measurement of catalytic activity

The catalytic performances of the supported catalysts were determined using a continuous flow reaction system under ambient pressure. For this purpose, catalyst powder (200mg) is granulated with 250 ÷ 450 µm under compressor pressure and placed between quartz reactor (370 mm height, 5 mm ID). A gas mixture of methane (CH_4), oxygen (O_2), and nitrogen (N_2) was introduced to the reactor after passing through a mixer, and the total flow of this gas mixture was fixed at 105mL/min, corresponding to a gas-hourly space velocity (GHSV) of 50,000 h^{-1} determined at 25 °C and 1.5 bar pressure. Catalysis was performed under a gas mixture of CH_4, O_2, N_2, in which molar ratio

(CH_4)/(O_2) = 4/1 (mol/mol). The reaction was at 850 °C, 900 °C, 950 °C, and reaction products were analyzed GC online coupled with Thermo Conductivity Detector and Flame Ionized Detector on TRACE GC ULTRA system.

The conversion of CH_4 was defined as:

$$\text{Conv (\%)} = \frac{A_{CH\,4total} - A_{CH\,4}}{A_{CH\,4total}} \times 100\%$$

Where: Conv (%): Conversion of CH_4

$A_{CH4total}$: Area of bypass peak of CH_4

A_{CH4}: Area of the remained peak of CH_4 after the reaction

Concentrations of C_2H_6, C_2H_4

$$C_{C2Hx} = \frac{A_{C_2H_x} \cdot C^*_{C_2H_x}}{A^*_{C_2H_x}}$$

Where: C^*_{C2Hx} is the concentration, and A^*_{C2Hx} is the corresponding peak area of the standard gas flow C_2H_x

Concentrations of CO_x: Determined through a standard curve between the concentration and the area of the corresponding GC peak

C_2H_x selectivity (%):

$$C_{C2Hx} = \frac{C2Hx}{C_{C_2H_4} + C_{CO_x} + C_{C_2H_6}} \text{x } 100\%$$

Results and discussion

Characterization of samples

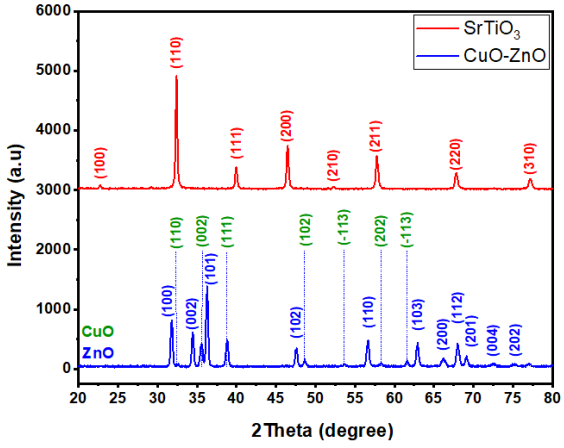

Figure 1: XRD pattern of $SrTiO_3$, CuO-ZnO catalysts

The X-ray diffraction patterns of the $SrTiO_3$ catalyst sample synthesized by the sol-gel and CuO-ZnO by the co-precipitation method are shown in Figure 1. The results show that in the $SrTiO_3$ sample, the diffraction peaks at 2θ angle are 22.76°, 32.38°, 39.94°, 46.46°, 52.4°, 57.74°, 67.78°, 72.5°, 77.12° and correspond to the crystal planes (100), (110), (111), (200), (210), (210), (211), (220), (300), (310). The observed peak positions and diffraction pattern matches with the JCPDS (Card No: 01-084-0443) data of $SrTiO_3$ compound having space group Pm-3m, which indicates the single phased cubic perovskite structure of the prepared compound [13].

For the CuO-ZnO sample, there are CuO feature planes with characteristic peaks at 2θ angles of 32.8°, 35.5°, 38.8°, 48.7°, 52.6°, 58.4°, 61, 6°, 66.2°, 68.1°, 72.5°, 75.2°, corresponding to (110), (002), (200), (-202), (020), (202), (-113) [14]. Furthermore, ZnO of the diffraction peaks at 2θ is 31.74° (100), 34.34° (002), 36.16° (101), 47.56° (102), 56.54° (110), 62.82° (103), 66.48° (200), 67.96° (112), 69.02° (201) represent hexagons of the wurtzite structure of ZnO, following JCPDS (Card No: 36 -1451) [15,16]. The peaks are pretty sharp, indicating that the samples have good crystallinity and no impurities.

Table 1: BET analysis of $SrTiO_3$ and CuO-ZnO

Adsorbent	BET Specific Surface area (m^2/g)
$SrTiO_3$	16.0
CuO-ZnO	0.76

Table 1 shows that the $SrTiO_3$ sample has a significantly higher surface area than CuO-ZnO when setting the value up to 16 m^2/g. This may be due to sintering on the oxide surface due to the sample heating temperature at 900 °C on a CuO-ZnO sample.

The SEM images show that the crystal structure of $SrTiO_3$ (Figure 2) is irregular. These crystals are rod-shaped with a length of 1-3 μm. The bottom diameter is about 0.5 μm. For CuO-ZnO, the crystalline particles have irregular cubic structures, size from 1-5 μm; The particles seem to aggregate with some other particles (the boundaries between the crystals were still observed) to create larger blocks. This may be due to the sintering taking place on the surface. To cause severe degradation of the specific surface of the catalyst, this is in agreement with the specific surface measurement results in Table 1.

https://doi.org/10.51316/jca.2022.060

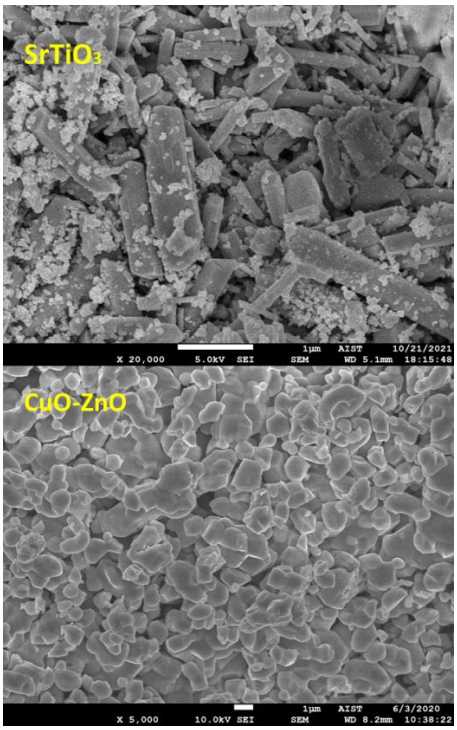

Figure 2: SEM image of $SrTiO_3$, CuO-ZnO

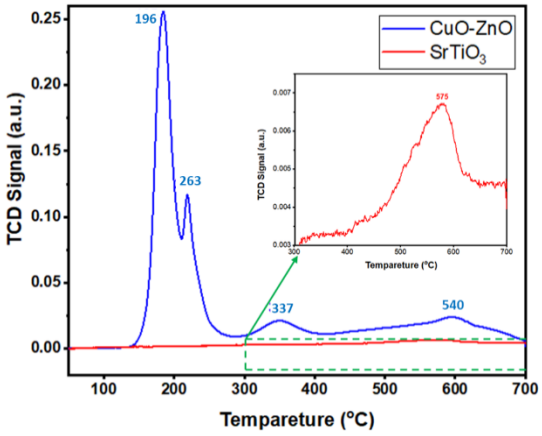

Figure 3: H_2-TPR profiles of the catalysts

Table 2: Quantification of H_2 consumption by peak integration of H_2-TPR profiles of $SrTiO_3$ and CuO-ZnO

Sample	The temperature at Maximum (°C)	Quantity (mmol/g)
CuO-ZnO	196	0.83
	263	1.5
	337	0.69
	540	1.31
$SrTiO_3$	575	6.58 x10^{-2}

To analyze the extent of reduction in the as-prepared $SrTiO_3$ and CuO-ZnO, temperature-programmed reduction (TPR) was performed in the same H_2 flow over 100 mg of the material. The signal corresponding to H_2 consumption is plotted against temperature and shown in Figure 3. CuO-ZnO showed two reduction peaks recorded at about 196 and 263 °C, corresponding to the reduced CuO and Cu_2O [17]. Furthermore, the remaining two peaks at 337 °C and 540 °C can reduce Cu^{2+} to Cu^{+} and Zn^{2+} to Zn [18]. The lower reduction temperature exhibited by 30% CuO-ZnO is a clear indication of the enhanced reduction potential of the CuO and ZnO species. For sample $SrTiO_3$ without reduction peak was recorded at temperatures below 400 °C. However, broad wide, and the small peak is seen in the temperature range of 500–700 °C, indicating a small, reducing capacity of the material. The only possible reduction in this system is the reduction of titanium ($Ti^{4+} \rightarrow Ti^{3+}$) with simultaneous removal of oxygen from the perovskite structure [19].

Table 2 shows that the H_2 quantification ion on the CuO-ZnO sample is superior to that of $SrTiO_3$. This shows that the reducing property of CuO-ZnO is better than that of $SrTiO_3$.

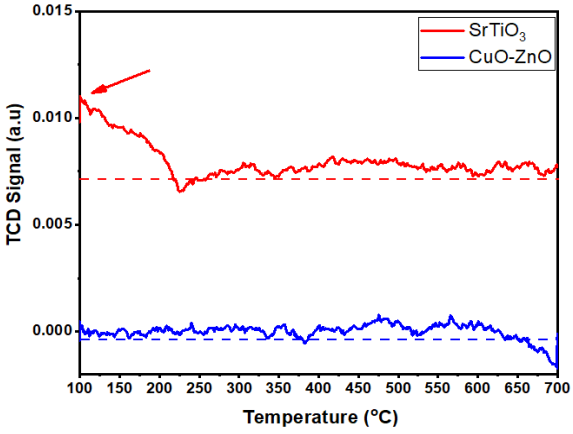

Figure 4: NH_3-TPD profiles of the catalysts

There are an unique feature in NH_3-TPD temperature-program gram desorption) patterns of $SrTiO_3$ and CuO-ZnO, as illustrated in Figure 4. The NH_3 desorption peak was detected at a temperature lower than 200 °C on $SrTiO_3$, which infers that some weak acidic sites are present on the catalyst surface. On the other hand, no peak was recorded on CuO-ZnO, proving that no acidic sites are available on this catalyst.

https://doi.org/10.51316/jca.2022.060

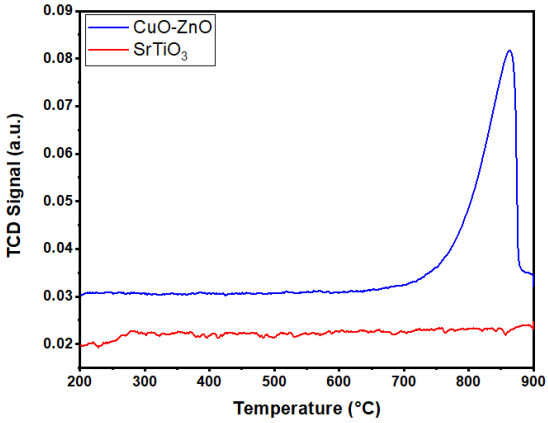

Figure 5: O_2-TPD profiles of the catalysts

The temperature-programmed desorption of O_2 (O_2-TPD) was performed to probe the active surface sites of the catalysts for oxygen adsorption/desorption. The results represent an O_2 loss peak at over 800 °C on CuO-ZnO, and no peak was recorded for $SrTiO_3$. This can be thought of as lattice oxygen loss (O_{lat}), the mighty chemisorbed O^- escaping from the copper cations [20]. This means that it exhibits better O_{lat} mobility on the CuO-ZnO sample than the other catalyst.

Bandgap energy is defined in Figure 6. The results show that the sample $SrTiO_3$ has an energy value of 3.18 eV, and CuO-ZnO is 2.65 eV. These values are all lower than the bandgap energies of ZnO (3.25 eV), TiO_2 (3.3 eV), which are attributed to the formation of oxygen vacancies on the catalyst surface, leading to the shift of light absorption peaks in the UV region (corresponding to enormous bandgap energy) to the visible light region (lower bang energy region) [21]. This could be because both catalysts have oxygen vacancies. However, there is not enough basis to compare this amount, the ability to create oxygen vacancy present between the two catalysts.

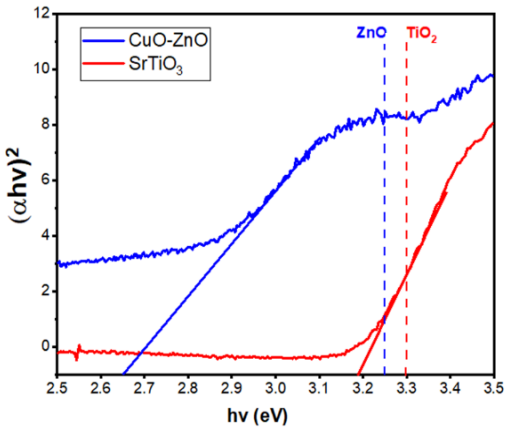

Figure 6: The bandgap energy of the catalysts

Catalytic activity

The catalysts were employed for the OCM reaction in the temperature range from 700 to 800 °C. The results in Figure 7 show that the reaction temperature has a great influence on the activity of the catalyst. As the reaction temperature increased, the CH_4 conversion of the catalyst samples increased rapidly. In which CuO-ZnO (increasing from 15% to 30%) is always higher than $SrTiO_3$ (8% → 15%). As for the selectivity of the C_2H_4 product, it is interesting that the CuO-ZnO catalyst produces mainly CO_x. Nevertheless, there is a tendency to collect more C_2 products as the temperature increases. It is possible that the optimum temperature point for obtaining product C_2 for this catalyst is above the rated temperature range. For $SrTiO_3$ this value is about 0.8% at 800 °C. This result is consistent with the characteristic properties of H_2-TPR and O_2-TPD of CuO-ZnO catalyst because they exhibit strong reducing and oxidizing properties leading to deep oxidation of CH_4 to CO_2 in the investigated temperature range.

In previous studies, the proposed mechanism for OCM reaction usually involves the formation of methyl radicals (CH_3*) via hydrogen abstraction from the methane by the active surface oxygen species available on the oxide catalyst surface [22, 23]. The methyl radicals then couple in the gaseous phase to form ethane (C_2H_6) which finally dehydrogenates to form the ethylene (C_2H_4). Indubitably, the concentration of the oxygen vacancy (O_{vac}) of oxide catalysts, especially at a high temperature, can be translated directly to the abundance of its lattice oxygen coupled with how readily available they are for reaction. Consequently, efficient OCM catalysts should have a high concentration of oxygen vacancy at temperatures typical of OCM reaction. From the UV-vis results, it can be shown that O_{vac} can exist on both catalysts, but the C_2H_4 formation efficiency of CuO-ZnO is extremely low compared to that of $SrTiO_3$. It is possible that besides the high selectivity for CO_x on the CuO-ZnO sample, it may also be influenced by the minimal surface area of this catalyst. This leads to the limitation of the number of oxygen vacancies and the ability of the material to contact the catalyst.

The mixture of product C_2 after reaction at 800 °C was analyzed by the GC system and compared the amount of product of C_2H_4 with C_2H_6, and the results are shown in Figure 8. The two samples present that the product ratio of C_2H_4 is much higher than that of C_2H_6. At the same time, CuO-ZnO gives this ratio higher

(84%) than $SrTiO_3$ (69%). This may be due to the strong redox properties of CuO-ZnO and the existence of weak acid sites on $SrTiO_3$ through NH_3-TPD analysis, leading to the reduction of C_2H_6 to C_2H_4.

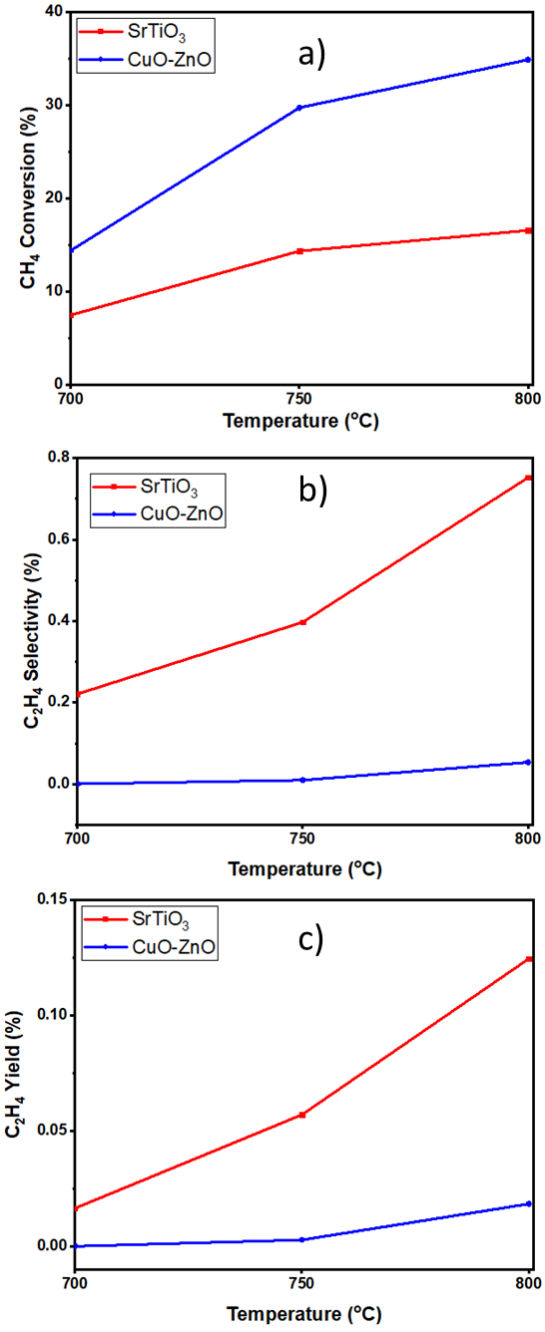

Figure 7: Catalytic activities of catalysts for the OCM reactions in the presence of oxygen

The $SrTiO_3$ catalyst in Figure 9 was pre-reacted granules with sizes from 250 ÷ 450 µm, and the reaction was carried out. Interestingly, after the reaction appeared a black layer that partially covered the catalyst, there may have been coke formation on the catalyst surface. This is consistent with the results of NH_3-TPD when on the surface of the $SrTiO_3$ catalyst, there are weak acid centers, which will promote the de-hydrocarbons to form coke.

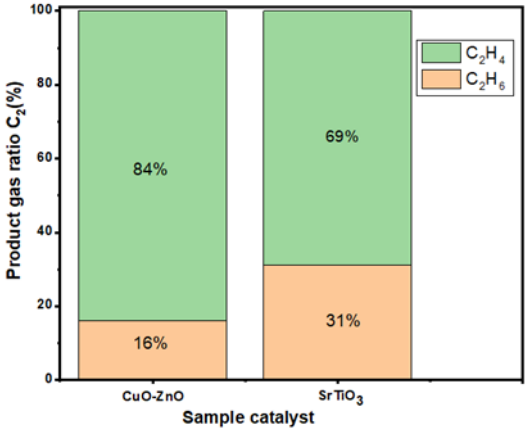

Figure 7: Compare the ratio of products C_2H_4 and C_2H_6 in a mixture of products C_2

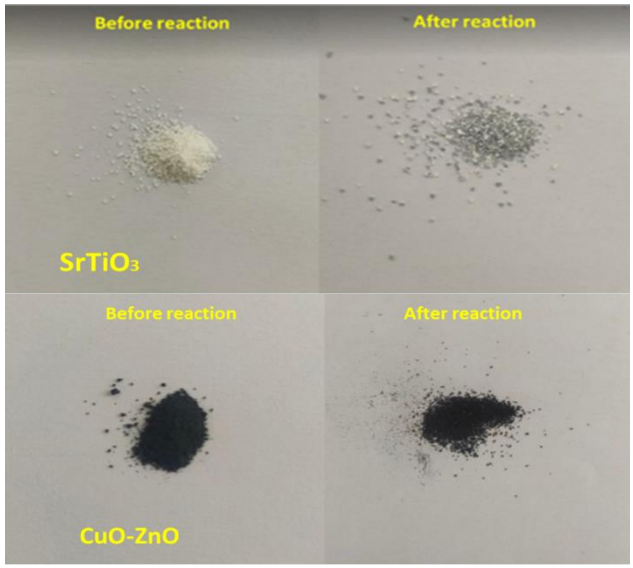

Figure 8: $SrTiO_3$, CuO-ZnO catalyst before and after the reaction

Conclusion

$SrTiO_3$ and CuO-ZnO samples were prepared and characterized to understand their properties. The formation of delicate crystalline phases is shown on the XRD of the two samples. However, due to the influence of sintering, the specific surface of CuO-ZnO is smaller than that of $SrTiO_3$, thereby reducing the active sites as well as the contact with the material gas.

The results showed that conversion the rate in the SrTiO3 sample was high (about 35%) at 850 °C, and form the product C_2H_4 with an yield of 0.12%. There

are an unique feature in NH_3-TPD (temperature-program gram desorption) patterns of $SrTiO_3$ and CuO-ZnO, as illustrated in Figure 4. The NH_3 desorption peak was detected at a temperature lower than 200 ^oC on $SrTiO_3$, which infers that some weak acidic sites are present on the catalyst surface. On the other hand, no peak was recorded on CuO-ZnO, proving that no acidic sites are available on this catalyst.

The SEM images also record sintering on CuO-ZnO, with the recorded structure of $SrTiO_3$ being mostly rod-shaped. The reduction and mobility of oxygen in the catalyst were also investigated through H_2-TPR and O_2-TPD, showing the superiority in the CuO-ZnO sample when the reduction peaks and O_2 depletion appeared, respectively.

Moreover, this may be why the product of choice for the OCM reaction in this catalyst sample is CO_x. In addition, coke formation on the $SrTiO_3$ catalyst was also noted, possibly as a by-product of the process due to weak acidic sites on $SrTiO_3$ by NH_3-TPD analysis. The proportions of products C_2H_4 and C_2H_6 were also considered; the results showed that a large proportion of products skewed towards C_2H_4.

Acknowledgments

This work has been supported by the RoHan Project funded by the German Academic Exchange Service (DAAD, No. 57315854) and the Federal Ministry for Economic Cooperation and Development (BMZ) inside the framework "SDG Bilateral Graduate school programme"
The authors thank the supports of Rohan project, DAAD, BMZ, GeViCat center, HUST.

References

1. Keller, G. E., M. M. Journal of Catalysis 73.1 (1982) 9-19. https://doi.org/10.1016/0021-9517(82)90075-6
2. Enger, B.C., Lødeng, R. and Holmen, A. Applied Catalysis A: General 346.1-2 (2008) 1-27. https://doi.org/10.1016/j.apcata.2008.05.018
3. Pereñíguez, R., González-DelaCruz, V. M., Holgado, J. P., & Caballero, A. Applied Catalysis B: Environmental 93.3-4 (2010) 346-353. https://doi.org/10.1016/j.apcatb.2009.09.040
4. Beck, B., Fleischer, V., Arndt, S., Hevia, M. G., Urakawa, A., Hugo, P., & Schomäcker, R. Catalysis Today 228 (2014) 212-218. https://doi.org/10.1016/j.cattod.2013.11.059
5. Lomonosov, V. I., and M. Yu Sinev. Kinetics and Catalysis 57.5 (2016) 647-676. https://doi.org/10.1134/S0023158416050128
6. Labinger, Jay Ay. Catalysis letters 1.11 (1988) 371-375. https://doi.org/10.1007/BF00766166
7. Arndt, S., Laugel, G., Levchenko, S., Horn, R., Baerns, M., Scheffler, M., ... & Schomäcker, R. Catalysis Reviews 53.4 (2011) 424-514. https://doi.org/10.1080/01614940.2011.613330
8. Kim, I., Lee, G., Na, H. B., Ha, J. M., & Jung, J. C . Molecular Catalysis 435 (2017) 13-23. https://doi.org/10.1016/j.mcat.2017.03.012
9. Li, S., Xu, N., Shi, J., Hu, M. Z. C., & Payzant, E. A . Journal of materials science letters 20.17 (2001) 1631-1633. https://doi.org/10.1023/A:1017966330832
10. Lim, S., Choi, J. W., Suh, D. J., Song, K. H., Ham, H. C., & Ha, J. M . Journal of catalysis 375 (2019) 478-492. https://doi.org/10.1016/j.jcat.2019.04.008
11. Lim, S., Choi, J. W., Suh, D. J., Song, K. H., Ham, H. C., & Ha, J. M . *Catalysis Today 352* (2020) 127-133. https://doi.org/10.1016/j.cattod.2019.11.014
12. Lim, S., Choi, J. W., Suh, D. J., Lee, U., Song, K. H., & Ha, J. M. Molecular Catalysis 489 (2020) 110925. https://10.1016/j.mcat.2020.110925
13. Padmini, E., K. Ramachandran. Solid State Communications 302 (2019) 113716. https://doi.org/10.1016/j.ssc.2019.113716
14. Kumari, V., Yadav, S., Jindal, J., Sharma, S., Kumari, K. and Kumar, N. Advanced Powder Technology (2020). https://doi.org/10.1016/j.apt.2020.04.033
15. Hsu, K.C., Fang, T.H., Hsiao, Y.J. and Li, Z.J . Journal of Alloys and Compounds (2020) 157014. https://doi.org/10.1016/j.jallcom.2020.157014
16. Ruan, S., Huang, W., Zhao, M., Song, H. and Gao, Z.. Materials Science in Semiconductor Processing 107 (2020) 104835. https://doi.org/10.1016/j.mssp.2019.104835
17. Aboul-Fotouh, Sameh MK. Journal of Fuel Chemistry and Technology 42.3 (2014) 350-356. https://doi.org/10.1016/S1872-5813(14)60020-7
18. Donphai, W., Piriyawate, N., Witoon, T., Jantaratana, P., Varabuntoonvit, V. and Chareonpanich, M.

19. Journal of CO_2 Utilization 16 (2016) 204-211. https://doi.org/10.1016/j.jcou.2016.07.007
20. Łącz, Agnieszka, and Ewa Drożdż. Journal of Solid State Electrochemistry 23.10 (2019) 2989-2997. https://doi.org/10.1007/s10008-019-04386-3
21. Kang, R., Ma, P., He, J., Li, H., Bin, F., Wei, X., Dou, B., Hui, K.N. and San Hui, K. Proceedings of the Combustion Institute (2020). https://doi.org/10.1016/j.proci.2020.06.186
22. Lim, S., Choi, J.W., Suh, D.J., Lee, U., Song, K.H. and Ha, J.M. Applied Cat alysis B: Environmental 264 (2020) 118554. https://doi.org/10.1016/j.apcatb.2019.118554
23. Beck, B., Fleischer, V., Arndt, S., Hevia, M.G., Urakawa, A., Hugo, P. Schomäcker, R. Catalysis Today 228 (2014) 3w212-218. https://doi.org/10.1016/j.cattod.2013.11.059
24. Kim, I., Lee, G., Na, H.B., Ha, J.M. Jung, J.C. Molecular Catalysis 435 (2017) 13-23. https://doi.org/10.1016/j.mcat.2017.03.012